Journal of Computational Physics 227 (2008) 10178–10195

Contents lists available at ScienceDirect

Journal of Computational Physics

journal homepage: www.elsevier.com/locate/jcp

A variational level set method for the topology optimization of steady-state Navier–Stokes flow

Shiwei Zhou, Qing Li *

School of Aerospace, Mechanical and Mechatronic Engineering, The University of Sydney, Sydney, NSW 2006, Australia

ARTICLE INFO

Article history:
Received 8 November 2007
Received in revised form 3 August 2008
Accepted 22 August 2008
Available online 5 September 2008

Keywords:
Topology optimization
Level set method
Variational method
Navier–Stokes flow
Maximum permeability
Minimum energy dissipation

ABSTRACT

The smoothness of topological interfaces often largely affects the fluid optimization and sometimes makes the density-based approaches, though well established in structural designs, inadequate. This paper presents a level-set method for topology optimization of steady-state Navier–Stokes flow subject to a specific fluid volume constraint. The solid-fluid interface is implicitly characterized by a zero-level contour of a higher-order scalar level set function and can be naturally transformed to other configurations as its host moves. A variational form of the cost function is constructed based upon the adjoint variable and Lagrangian multiplier techniques. To satisfy the volume constraint effectively, the Lagrangian multiplier derived from the first-order approximation of the cost function is amended by the bisection algorithm. The procedure allows evolving initial design to an optimal shape and/or topology by solving the Hamilton–Jacobi equation. Two classes of benchmarking examples are presented in this paper: (1) periodic microstructural material design for the maximum permeability; and (2) topology optimization of flow channels for minimizing energy dissipation. A number of 2D and 3D examples well demonstrated the feasibility and advantage of the level-set method in solving fluid–solid shape and topology optimization problems.

1. Introduction

Design of fluid fields signifies one class important yet challenging issue in physics. Due to its mathematical and physical complexity, the solutions to such problems often necessitate various sophisticated numerical algorithms. Since Pironnea's pioneering work in 1970s [1,2] substantial attention has been paid to shape optimization for incompressible viscous flow for its obvious theoretical and practical values, which have led to a great body of publications over the last three decades [3,4]. In this respect, the boundary represented shape optimization and density-based topology optimization have symbolized two most intuitive and prevalent methods for fluid design problems. Their applications can be found from coast engineering [5], to automotive, naval and aerospace engineering [6–8]. However, the shape optimization lacks an important function in identifying new topologies and does not guarantee an overall optimum, and the density-based topology optimization often generates non-smooth interfaces, leading to inaccurate representation of the fluid boundaries. More importantly, it is by no means easy to formulate these two optimization methods in a unified framework, thus causing difficulties in a coupled shape and topological design scenario [3].

The topological variation in shape optimization of fluid fields has been a topic of research since Tartar's work in 1974 [9]. A critical problem is how to seek for an optimal topology so that new boundaries can be developed. In this respect, Steven et al. [10] introduced an element (density) based topology-shape optimization method for the steady incompressible fluid

* Corresponding author. Tel.: +61 2 9351 8607; fax: +61 2 9351 7060.
E-mail address: Q.Li@usyd.edu.au (Q. Li).

0021-9991/$ - see front matter Crown Copyright © 2008 Published by Elsevier Inc. All rights reserved.
doi:10.1016/j.jcp.2008.08.022

design in the Stokes flow, in which a simple but effective procedure named evolutionary structural optimization (for short, ESO) [11] was adopted. Late, a more sophisticated study on fluid optimization, including the existence of solution and convergence of algorithm, was conducted by Borrvall and Petersson [12]. They proposed an artificial "inverse permeability" that is proportional to the elemental thickness of a two-dimensional channel with Navier–Stokes flow. To ensure the nonexistence of intermediate thickness (density), the variable is also penalized by a positive factor, very similar to the solid isotropic material with penalization (SIMP) method in structural topology optimization [13]. This model was further extended to the shape optimization of fluid fields governed by the static Navier–Stokes and Darcy–Stokes flow, and a series of novel fluid configurations with minimal dissipation energy were obtained [14–16].

As a relatively newer numerical technique, the level set method pioneered by Osher and Sethian [17] provides a powerful computing tool for tracking dynamically-changing interfaces. Its breadth of applications have been extensively evidenced in computational geometry [18], image processing [19], structural optimization [20–22], computer-aided material design [23,24], inverse problems involving obstacles [25,26], fluid mechanics [27,28] and more [29,30]. Of these applications, structural optimization gains increasing attention in recent years. In this regard, a breakthrough was made by Sethian and Wiegmann [20], who demonstrated the possibility of the level set method on solving topology optimization of elastic structures. In their earlier study, a non-gradient parameter like the von Mises stress was adopted as the driving velocity. In order to incorporate shape sensitivity into the level set method, Osher and Santosa [31] tackled a vibration problem by acquiring optimal resonant frequency subject to geometric constraints. Allaire et al. [22] further encompassed the classical material derivatives into the level-set method and exhibited a new prospective of using shape sensitivity to drive topology optimization.

A more comprehensive and systematic study on the level set based topology optimization was performed by Wang et al. [21]. By means of the Fréchet derivative a sensitivity based velocity was formulated in terms of the displacement field, in which a Lagrange multiplier was used to incorporate volume constraints. This work played an important role on demonstrating the capability of the level-set technique in solving a broad range of topology optimization problems. The further studies allow formulating material derivatives for linear and nonlinear elasticities [22,32] that enable a more general topological optimization. Later, the level set model was developed in a framework of radial basis function [33], where the motion of the interfaces is dominated by ordinary differential equations and the optimization can evolves smoothly without the need of reinitialization in each iteration.

One major advantage of the level-set method lies in analyzing the continuously-moving interfaces between adjacent phases, thereby ensuring a smooth topological boundary. Unlike those prevalent density-based algorithms, e.g. SIMP [12,14,15] and ESO [10] that lack mathematical representation of material interfaces involved, the level-set method adopts a "region-based representation" with explicit function. It was successfully used to trace the interface motion of multiphase flow governed by the Navier–Stokes equations [27,28], and exhibited superior suitability to represent fluid-fluid and fluid–solid interfaces mathematically.

With substantial success in the applications of level set method to structural optimization and fluid mechanics modeling, the question is whether it is possible to develop a level-set based topology optimization for fluid materials and structures. In this context, Jung et al. [34] explored one kind of velocity for the level set function with variational method and yielded a series of triply-periodic minimal surfaces, which separate the phases of a composite into bicontinuous structures in 3D space. In addition to such composites with one or two extreme physical properties [35], Jung and Torquato [34] found that when substituting one solid phase with fluid, the structures divided by the Schwartz P minimal surface (the surface with minimal surface area) make the permeability of porous media maximum, thus leading to a conjecture that the permeability is inversely proportional to the solid-fluid contacting area. More recently, Duan et al. [36] attempted the shape optimization of fluids with the level set method, where the Gateaux shape derivative was used to analyze the sensitivity of the objective function.

In this paper, we generalize the level set method for the fluidic topology optimization in a number of ways. Firstly, the level-set method will be addressed in a unified framework for both shape and topology optimization where an implicit expression of the fluid–solid interface is determined via the zero-level contour of a higher-dimensional level-set function. As a specific application, the topological and shape optimization is presented for permeable microstructural materials composed of periodic base cells, which has not been well studied in the level-set method yet, despite its popularity in various density-based techniques [37]. Secondly, the normal velocity of the level set function is derived by combining the variational analysis of the cost function with the adjoint variable method. Unlike traditional mean compliance problem in structural topology optimization, the design problems considered in this paper might not be self-adjoint (the adjoint variables used in the normal velocity of the level set function are different from the solutions to the state equation). Thus we need to solve the adjoint equation of the Navier–Stokes equation, making the algorithm more complicated and time-consuming. Thirdly, we attempt to tackle some relevant numerical issues when implementing the level-set method, which include the bisection technique [33,38] to regulate the volume fraction, the remeshing of the fluid domain and the reinitialization of the level set function.

2. Level set models in fluid topology optimization

2.1. Boundary expression with level set models

In traditional density-based structural optimization methods, topological boundaries are represented by the nucleation and separation of compositional phases. However, adequate solidification cannot be always guaranteed within a small band

close to the boundary even with large exponential penalty on the design variable of relative density, thus leading to ambiguous or blur interface. The level set method originally proposed by Osher and Sethian in [17] is however based upon a simple expression of the implicit boundary corresponding to the zero-level contour of a higher-dimensional scalar function $\phi(\mathbf{x})$. It appears more flexible to formulate the coalescence and separation of interface via moving level set function $\phi(\mathbf{x})$ along its normal direction with given velocity. The suitability of the level set methods to the structural topology optimization was demonstrated in a series of recent studies, and an extensive impact has been made on traditional structural optimization community [20–22].

Without loss of generality, we would like to take a periodic base cell model as an example (Fig. 1(b)) to formulate the fluidic optimization problem here. Mathematically, the values of the Lipschitz-continuous level set function $\phi(\mathbf{x})$ (Fig. 1(a)) define a zero-level contour (interface) ($\Gamma = \{\mathbf{x}:\mathbf{x} \in \Omega,\ \varphi(\mathbf{x}) = 0\}$) by separating its outside/inside domain (Ω_1/Ω_2 in Fig. 1(b)) as follows:

$$\varphi(\mathbf{x}) < 0 \quad \forall \mathbf{x} \in \Omega_2 \setminus \Gamma, \tag{1}$$

$$\varphi(\mathbf{x}) > 0 \quad \forall \mathbf{x} \in \Omega_1 \setminus \Gamma, \tag{2}$$

where $\Omega = \Omega_1 \cup \Omega_2$ denotes a reference design domain, and $\Gamma = \Gamma_0 \cup \Gamma_1 \cup \cdots \Gamma_4$ and $\Gamma_i \cap \Gamma_j \neq \emptyset$; $i,j = 0, \ldots, 4$; $i \neq j$ represents the boundary of the base cell model, which repeats periodically in space to constitute the scaffold with the maximum isotropic permeability. This problem can be modeled with one input (Γ_1) and one output (Γ_2) boundary on the left and right edges, and two periodic boundaries Γ_3 and Γ_4 on the top and bottom edges [39], which constitute the Neumann's boundaries $\Gamma_N = \Gamma_1 \cup \Gamma_2$ and periodic boundaries $\Gamma_P = \Gamma_3 \cup \Gamma_4$, respectively. To accommodate general optimization algorithms, the maximum permeability problem is regarded as a minimization of its negative values.

2.2. Level set models in fluid topology optimization

In the abovementioned fluid topology optimization, the velocity $\mathbf{u}$ and pressure p fields are the solutions to the steady state dimensionless Navier–Stokes equations that govern the incompressible Newtonian fluids in Ω_2, as

$$\begin{aligned} &-\mu\nabla^2\mathbf{u} + (\mathbf{u}\cdot\nabla)\mathbf{u} + \nabla p = \mathbf{f} \quad \forall \mathbf{x} \in \Omega_2 \\ &-\operatorname{div}\mathbf{u} = 0 \qquad \forall \mathbf{x} \in \Omega_2, \\ &\mathbf{u} = 0 \quad \forall \mathbf{x} \in \Gamma_0, \\ &\boldsymbol{\sigma}\mathbf{n} = \mathbf{g} \quad \forall \mathbf{x} \in \Gamma_N \\ &\mathbf{u}, p|_{\Gamma_3} = \mathbf{u}, p|_{\Gamma_4}. \end{aligned} \tag{3}$$

The dependence of the variables on $\mathbf{x}$ is not shown in this and following formulae for brevity. The Cauchy stress tensor $\boldsymbol{\sigma}$ is defined by $\boldsymbol{\sigma}(\mathbf{u},p) = \mu\nabla\mathbf{u} - p\mathbf{I}$ and the nonlinear convective term is given as $(\mathbf{u}\cdot\nabla)\mathbf{u} = \sum_{i=1}^{2} u_i \frac{\partial}{\partial x_i}\mathbf{u}$. $\nabla^2\mathbf{u}$ denotes the Hessian matrix of $\mathbf{u}$ in a classical sense. The reciprocal of Reynolds number, vector-valued external force fields per unit mass and surface tractions are denoted by μ, $\mathbf{f}$ and $\mathbf{g}$, respectively. The boundary of fluids should be Lipschitz continuous with the general requirements for the level set function.

The cost function to be minimized in the optimization problems often takes an integral form over the fluid domain Ω_2 along its boundary Γ, given by

$$\min D(\mathbf{u}) = \int_{\Omega_2} A(\mathbf{u})\,\mathrm{d}\mathbf{x} + \int_{\Gamma} B(\mathbf{u})\,\mathrm{d}\mathbf{s}. \tag{4}$$

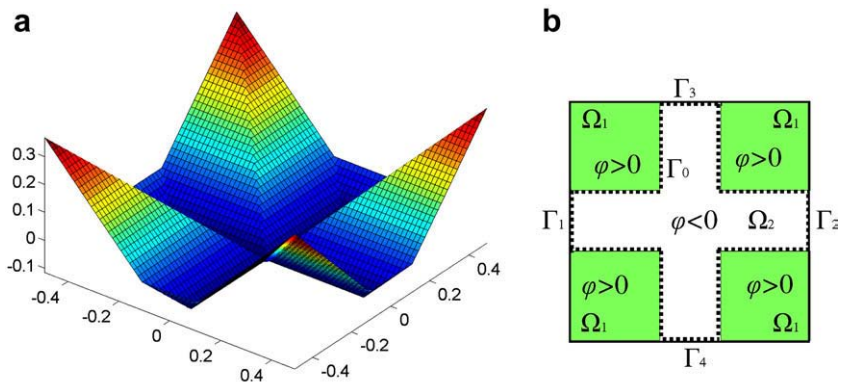

Fig. 1. Expression of the boundaries in a base cell model of periodic composite (a) the level set function $\phi(\mathbf{x})$ and (b) the isosurface at zero-level plane.

For the periodic base cell problem illustrated in Fig. 1(b), a special attention is paid to the non-slipping boundary Γ_0, on which the boundary integrals can be converted to volume integrals over the entire domain Ω as [34]

$$\int_{\Gamma_0} B(\mathbf{u})\,\mathrm{d}\mathbf{s} = \int_{\Omega} \tau(\varphi)\|\nabla\varphi\|B(\mathbf{u})\,\mathrm{d}\mathbf{x}. \tag{5}$$

In the level set framework, the problem of fluid topology optimization can be thus formulated in terms of the level set function $\varphi(\mathbf{x})$ as,

$$\begin{aligned} \underset{\Gamma_0}{\text{Minimize}} \quad & D(\mathbf{u},\varphi) = \int_{\Omega} H(-\varphi)A(\mathbf{u})\,\mathrm{d}\mathbf{x} + \int_{\Omega} \tau(\varphi)\|\nabla\varphi\|B(\mathbf{u})\,\mathrm{d}\mathbf{x} \\ \text{subject to} \quad & \int_{\Omega} H(-\varphi)\,\mathrm{d}\mathbf{x} \leqslant V_0 \\ & a(\mathbf{u},\mathbf{v})_{\Omega_2} + b(\mathbf{u};\mathbf{u},\mathbf{v})_{\Omega_2} - (\mathrm{div}\mathbf{v},p)_{\Omega_2} = (\mathbf{f},\mathbf{v})_{\Omega_2}, \\ & -(\mathrm{div}\mathbf{u},q)_{\Omega_2} = 0, \\ & \mathbf{v} = 0 \quad \forall \mathbf{x} \in \Gamma_0, \end{aligned} \tag{6}$$

where V_0 is the volume constraint for the fluidic region, namely the maximum amount of fluid available in the design domain Ω and $\mathbf{v}$, q are the trial functions. The equalities in Eq. (6) describe the weak form of the Navier–Stokes equations with bilinear and trilinear forms $a(\mathbf{u},\mathbf{v})_{\Omega_2} = \mu\int_{\Omega} H(-\varphi)\nabla\mathbf{u}\cdot\nabla\mathbf{v}\,\mathrm{d}\mathbf{x}$, and $b(\mathbf{u};\mathbf{u},\mathbf{v})_{\Omega_2} = \int_{\Omega} H(-\varphi)(\mathbf{u}\cdot\nabla)\mathbf{u}\cdot\mathbf{v}\,\mathrm{d}\mathbf{x}$, respectively. The $L_2(\Omega)$ Lebesgue inner product is defined as $(\mathbf{u},\mathbf{v})_{\Omega_2} = \int_{\Omega} H(-\varphi)\mathbf{u}\cdot\mathbf{v}\,\mathrm{d}\mathbf{x}$. If the normal directions on the periodic boundaries Γ_3 and Γ_4 are opposite in the permeable material design, the boundary integrals along them will vanish when deriving the weak form of the Navier–Stokes equations with integration by parts. The Neumann boundaries are also implicitly included in the weak form. According to Eq. (6), the optimization problem becomes to determine the optimal solid/fluid interface boundary Γ_0 in terms of the minimization of the cost function $D(\mathbf{u},\varphi)$ in the given fluid volume governed by the static Navier–Static equations. In Eq. (6), the norm of the gradient of level set function is given as $\|\nabla\| = (\nabla\varphi\cdot\nabla\varphi)^{1/2}$, while the Heaviside function $H(\phi)$ is defined by

$$H(\varphi) = \begin{cases} 1 & \varphi \geqslant 0 \\ 0 & \varphi < 0 \end{cases} \tag{7}$$

and the Dirac function by $\tau(\varphi) = \frac{\mathrm{d}H(\varphi)}{\mathrm{d}\varphi}$.

The level set function is dynamically driven by a normal velocity in terms of the Hamilton–Jacobin equation given by

$$\frac{\partial\varphi}{\partial t} + \mathbf{V_n}\|\nabla\varphi\| = 0, \tag{8}$$

where $\mathbf{n} = \nabla\varphi/\|\nabla\varphi\|$ defines the unit normal. The normal velocity $\mathbf{V_n}$ plays an important role in evolving the level set function as it derives a proper contour in terms of the sensitivity of the cost function to be discussed below.

3. Sensitivity analysis and numerical issues

3.1. Sensitivity analysis

As discussed in the previous section, precise determination of the normal velocity is the key to the implementation of the level-set method. It is worthwhile mentioning that the Fréchet derivative was used by Wang et al. [21] to seek the optimal normal velocity for structural topology optimization. Similar results were obtained by Allaire et al. [22] with material derivative as developed by Murat and Simon in [40]. Recently, a variational level set method was proposed by Jung et al. [34] to handle the minimal surface problem. In view of its performance, we will extend it to fluid topology optimization. However, a simple reformulation [34] may not be feasible as the steady-state Navier–Stokes equations totally change the physical environments of the level set function. The adjoint variable method has to be used in such complex scenario, which needs a solution to the adjoint system of Navier–Stokes equations. For this purpose, we adopt a more general variational method as follows

With the consideration of volume constraint, the cost function in Eq. (4) becomes

$$D(\mathbf{u},\varphi,\lambda_0) = \int_{\Omega} (H(-\varphi)A(\mathbf{u}) + \tau(\varphi)\|\nabla\varphi\|B(\mathbf{u}))\,\mathrm{d}\mathbf{x} + \lambda_0\left(\int_{\Omega} H(-\varphi)\,\mathrm{d}\mathbf{x} - V_0\right) \tag{9}$$

by means of a Lagrange multiplier λ_0. The first order variation of this cost function gives

$$\delta D = \frac{\partial D}{\partial\varphi}\delta\varphi + \frac{\partial D}{\partial\lambda_0}\delta\lambda_0 + \frac{\partial D}{\partial\mathbf{u}}\delta\mathbf{u} = \delta_{\varphi}D + \delta_{\lambda_0}D + \int_{\Omega} (H(-\varphi)A'(\mathbf{u}) + \tau(\varphi)\|\nabla\varphi\|B'(\mathbf{u}))\delta\mathbf{u}\,\mathrm{d}\mathbf{x} \tag{10}$$

Furthermore, by considering the constraint of the steady-state Naiver–Stokes equations and boundary conditions, a more general objective function in terms of Lagrangian multipliers is defined by

$$R(\mathbf{u},p,\varphi,\mathbf{w},q)=\int_{\Omega}(H(-\varphi)A(\mathbf{u})+\tau(\varphi)\|\nabla\varphi\|B(\mathbf{u}))\,\mathrm{d}\mathbf{x}+a(\mathbf{u},\mathbf{w})_{\Omega_2}+b(\mathbf{u};\mathbf{u},\mathbf{w})_{\Omega_2}-(\mathrm{div}\,\mathbf{w},p)_{\Omega_2}-(\mathbf{f},\mathbf{w})_{\Omega_2}-(\mathrm{div}\,\mathbf{u},q)_{\Omega_2}+\int_{\Gamma_0}\mathbf{w}\cdot\mathbf{u}\,\mathrm{d}\mathbf{s} \tag{11}$$

where $(\mathbf{u},p,\varphi,\mathbf{w},q)\in(W_0^1(\Omega_2);L_0^1(\Omega_2);L^2(\Omega_2);W_0^1(\Omega_2);L_0^1(\Omega_2))$. The first order variation of the objective function Eq. (11) with respect to $\mathbf{u}$ gives

$$\delta_{\mathbf{u}}R=\int_{\Omega}(H(-\varphi)A'(\mathbf{u})+\tau(\varphi)\|\nabla\varphi\|B'(\mathbf{u}))\delta\mathbf{u}\,\mathrm{d}\mathbf{x}+a(\delta\mathbf{u},\mathbf{w})_{\Omega_2}+b(\delta\mathbf{u};\mathbf{u},\mathbf{w})_{\Omega_2}+b(\mathbf{u};\delta\mathbf{u},\mathbf{w})_{\Omega_2}-(q,\mathrm{div}(\delta\mathbf{u}))_{\Omega_2}+\int_{\Gamma_0}\mathbf{w}\cdot\delta\mathbf{u}\,\mathrm{d}\mathbf{s} \tag{12}$$

Continuing to integrate by part in Eq. (12) and considering the periodic boundary condition, one can derive the following equations,

$$\int_{\Omega}(H(-\varphi)A'(\mathbf{u})+\tau(\varphi)\|\nabla\varphi\|B'(\mathbf{u}))\delta\mathbf{u}\,\mathrm{d}\mathbf{x}=\int_{\Omega_2}A'(\mathbf{u})\delta\mathbf{u}\,\mathrm{d}\mathbf{x}+\int_{\Gamma_0}B'(\mathbf{u})\delta\mathbf{u}\,\mathrm{d}\mathbf{s} \tag{13}$$

$$a(\delta\mathbf{u},\mathbf{w})_{\Omega_2}=-\mu(\mathrm{div}(\nabla\mathbf{w}),\delta\mathbf{u})_{\Omega_2}+\mu(\nabla\mathbf{w}\mathbf{n},\delta\mathbf{u})_{\Gamma_0\cup\Gamma_N} \tag{14}$$

$$b(\mathbf{u};\delta\mathbf{u},\mathbf{w})_{\Omega_2}=-((\mathbf{u}\cdot\nabla)\mathbf{w},\delta\mathbf{u})_{\Omega_2}+((\mathbf{u}\cdot\mathbf{n})\mathbf{w},\delta\mathbf{u})_{\Gamma_0\cup\Gamma_N} \tag{15}$$

$$b(\delta\mathbf{u};\mathbf{u},\mathbf{w})_{\Omega_2}=(\mathbf{w}\nabla\mathbf{u},\delta\mathbf{u})_{\Omega_2} \tag{16}$$

$$(q,\mathrm{div}(\delta\mathbf{u}))_{\Omega_2}=-(\nabla q,\delta\mathbf{u})_{\Omega_2}+(q\mathbf{n},\delta\mathbf{u})_{\Gamma_0\cup\Gamma_N} \tag{17}$$

Inserting Eqs. (13)–(17) into Eq. (12) yields

$$\delta_{\mathbf{u}}R=\int_{\Omega_2}(A'(\mathbf{u})-\mu\mathrm{div}(\nabla\mathbf{w})-(\mathbf{u}\cdot\nabla)\mathbf{w}+\mathbf{w}\cdot\nabla\mathbf{u}+\nabla q)\delta\mathbf{u}\,\mathrm{d}\mathbf{x}+(B'(\mathbf{u})+\boldsymbol{\sigma}(\mathbf{w},q)\mathbf{n}+(\mathbf{u}\cdot\mathbf{n})\mathbf{w}+\mathbf{w},\delta\mathbf{u})_{\Gamma_0}+(\boldsymbol{\sigma}(\mathbf{w},q)\mathbf{n}+(\mathbf{u}\cdot\mathbf{n})\mathbf{w},\delta\mathbf{u})_{\Gamma_N} \tag{18}$$

Similarly, the first order variation of the objective function, Eq. (11), with respect to p gives

$$\delta_pR=-(\mathrm{div}\,\mathbf{w},\delta p) \tag{19}$$

If set $\delta\mathbf{u}\in W_0^1(\Omega_2)$ in Eq. (18) and consider the Kuhn–Tucker condition for the optimal value of the objective, $\delta_{\mathbf{u}}R=0$, the following equation can be derived.

$$-\mu\mathrm{div}(\nabla\mathbf{w})-(\mathbf{u}\cdot\nabla)\mathbf{w}+\mathbf{w}\cdot\nabla\mathbf{u}+\nabla q=-A'(\mathbf{u})\qquad\forall\mathbf{x}\in\Omega_2 \tag{20}$$

Plugging $\delta p=L_0^1(\Omega_2)$ in Eq. (19) and taking into account $\delta_pR=0$, one obtains

$$-\mathrm{div}\,\mathbf{w}=0\qquad\forall\mathbf{x}\in\Omega_2 \tag{21}$$

As $\delta\mathbf{u}\in W_0^1(\Omega_2)$, $\delta\mathbf{u}=0\ \forall\ \mathbf{x}\in\Gamma_0$ in Eq. (18) and considering $\delta_{\mathbf{u}}R=0$, the following relation holds

$$(\boldsymbol{\sigma}(\mathbf{w},q)\mathbf{n}+(\mathbf{u}\cdot\mathbf{n})\mathbf{w},\delta\mathbf{u})_{\Gamma_N}=0 \tag{22}$$

As a result of the combination of Eqs. (20)–(22) and considering $\mathbf{w}\in W_0^1(\Omega_2)$, the adjoint equations are given as,

$$\begin{aligned}&-\mu\mathrm{div}(\nabla\mathbf{w})-(\mathbf{u}\cdot\nabla)\mathbf{w}+\mathbf{w}\cdot\nabla\mathbf{u}+\nabla q=-A'(\mathbf{u})\qquad\forall\mathbf{x}\in\Omega_2\\&-\mathrm{div}\,\mathbf{w}=0\qquad\forall\mathbf{x}\in\Omega_2\\&\mathbf{w}=0\qquad\forall\mathbf{x}\in\Gamma_0\\&\boldsymbol{\sigma}(\mathbf{w},q)\mathbf{n}=-(\mathbf{u}\cdot\mathbf{n})\mathbf{w}\qquad\forall\mathbf{x}\in\Gamma_N\end{aligned} \tag{23}$$

In the meantime, the first order variation of the first equality of the weak form of the Navier–Stokes equations with respect to ϕ gives

$$a(\delta\mathbf{u},\mathbf{v})_{\Omega_2}+b(\delta\mathbf{u};\mathbf{u},\mathbf{v})_{\Omega_2}+b(\mathbf{u};\delta\mathbf{u},\mathbf{v})_{\Omega_2}-(\delta p,\mathrm{div}\,\mathbf{v})_{\Omega_2}=\int_{\Omega}H(-\varphi)\tau(\varphi)(a(\mathbf{u},\mathbf{v})+b(\mathbf{u};\mathbf{u},\mathbf{v})-(p,\mathrm{div}\,\mathbf{v})-(\mathbf{f},\mathbf{v}))\delta\varphi\,\mathrm{d}\mathbf{x} \tag{24}$$

Taking into account the adjoint variable $\mathbf{w}=0$, $\forall\mathbf{x}\in\Gamma_0$ in Eq. (12) and $\delta_{\mathbf{u}}R=0$, one can obtain

$$a(\delta\mathbf{u},\mathbf{w})_{\Omega_2}+b(\delta\mathbf{u};\mathbf{u},\mathbf{w})_{\Omega_2}+b(\mathbf{u};\delta\mathbf{u},\mathbf{w})_{\Omega_2}-(q,\mathrm{div}(\delta\mathbf{u}))_{\Omega_2}=-\int_{\Omega}(H(-\varphi)A'(\mathbf{u})+\tau(\varphi)\|\nabla\varphi\|B'(\mathbf{u}))\delta\mathbf{u}\,\mathrm{d}\mathbf{x} \tag{25}$$

Considering that the trial functions $\mathbf{v}$, p in Eq. (24) and the adjoint variable $\mathbf{w}$, q in Eq. (25) belong to the same functional space. Thus, one can make them equal such that the following equation can be derived if substitute $\mathbf{w}$ for $\mathbf{v}$ in Eq. (24)

$$\int_\Omega (H(-\varphi)A'(\mathbf{u}) + \tau(\varphi)\|\nabla\phi\|B'(\mathbf{u}))\delta\mathbf{u}\,d\mathbf{x} = -\int_\Omega H(-\varphi)\tau(\varphi)(a(\mathbf{u},\mathbf{w}) + b(\mathbf{u};\mathbf{u},\mathbf{w}) - (p,\mathrm{div}\,\mathbf{w}) - (\mathbf{f},\mathbf{w}))\delta\varphi\,d\mathbf{x}$$
$$= -\int_{\Gamma_0} \frac{1}{\|\nabla\phi\|}(a(\mathbf{u},\mathbf{w}) + b(\mathbf{u};\mathbf{u},\mathbf{w}) - (p,\mathrm{div}\,\mathbf{w}) - (\mathbf{f},\mathbf{w}))\delta\varphi\,d\mathbf{s} \tag{26}$$

Note that

$$\delta_\varphi\left(\int_\Omega H(-\varphi)A(\mathbf{u})d\mathbf{x}\right) = -\int_\Omega \tau(\varphi)\delta\varphi A(\mathbf{u})d\mathbf{x} = -\int_{\Gamma_0}\frac{\delta\varphi}{\|\nabla\varphi\|}A(\mathbf{u})\,d\mathbf{s} \tag{27}$$

$$\delta_\varphi\left(\lambda_0\left(\int_\Omega H(-\varphi)d\mathbf{x} - V_0\right)\right) = -\int_\Omega \lambda_0\tau(\varphi)\delta\varphi\,d\mathbf{x} = -\int_{\Gamma_0}\frac{\delta\varphi}{\|\nabla\varphi\|}\lambda_0\,d\mathbf{s} \tag{28}$$

$$\delta_{\lambda_0}\left(\lambda_0\left(\int_\Omega H(-\varphi)d\mathbf{x} - V_0\right)\right) = \int_\Omega \delta\lambda_0\left(\int_\Omega H(-\varphi)\,d\mathbf{x} - V_0\right)d\mathbf{x} \tag{29}$$

$$\begin{aligned}
\delta_\varphi\left(\int_\Omega \tau(\varphi)\|\nabla\varphi\|B(\mathbf{u})\,d\mathbf{x}\right) &= \int_\Omega (\tau'(\varphi)\delta\varphi\|\nabla\varphi\| + \tau(\varphi)\delta(\|\nabla\varphi\|))B(\mathbf{u})\,d\mathbf{x}\\
&= \int_\Omega \left(\tau'(\varphi)\delta\varphi\|\nabla\varphi\| + \tau(\phi)\frac{\nabla\varphi\cdot\nabla(\delta\varphi)}{\|\nabla\varphi\|}\right)B(\mathbf{u})\,d\mathbf{x}\\
&= \int_\Omega \left(\tau'(\varphi)\delta\varphi\|\nabla\varphi\| + \nabla\cdot\left(\delta\varphi\tau(\phi)\frac{\nabla\varphi}{\|\nabla\varphi\|}\right) - \delta\varphi\nabla\cdot\left(\tau(\varphi)\frac{\nabla\varphi}{\|\nabla\varphi\|}\right)\right)B(\mathbf{u})\,d\mathbf{x}\\
&= \int_\Omega \left(\tau'(\varphi)\delta\varphi\|\nabla\varphi\| + \nabla\cdot(\delta\phi\tau(\varphi)\mathbf{n}) - \delta\varphi\tau(\varphi)\nabla\cdot\mathbf{n} - \delta\varphi\tau'(\varphi)\frac{\nabla\varphi\cdot\nabla\varphi}{\|\nabla\varphi\|}\right)B(\mathbf{u})\,d\mathbf{x}\\
&= \int_\Omega (\tau'(\varphi)\delta\varphi\|\nabla\varphi\| + \nabla\cdot(\delta\varphi\tau(\varphi)\mathbf{n}) - \delta\varphi\tau(\varphi)\nabla\cdot\mathbf{n} - \delta\varphi\|\nabla\varphi\|\tau'(\varphi))B(\mathbf{u})\,d\mathbf{x}\\
&= \int_\Omega (\nabla\cdot(\delta\varphi\tau(\varphi)\mathbf{n}) - \delta\varphi\tau(\varphi)\nabla\cdot\mathbf{n})B(\mathbf{u})\,d\mathbf{x}\\
&= -\int_\Omega \delta\varphi\tau(\varphi)\frac{\partial B(\mathbf{u})}{\partial\mathbf{n}}\,d\mathbf{x} + \int_{\partial\Omega}\delta\varphi\tau(\varphi)B(\mathbf{u})\,d\mathbf{x} - \int_{\Gamma_0}\frac{B(\mathbf{u})\delta\varphi}{\|\nabla\varphi\|}\nabla\cdot\mathbf{n}\,d\mathbf{s}\\
&= -\int_{\Gamma_0}\left(B(\mathbf{u})\kappa + \frac{\partial B(\mathbf{u})}{\partial\mathbf{n}}\right)\frac{\delta\varphi}{\|\nabla\varphi\|}\,d\mathbf{s}
\end{aligned} \tag{30}$$

where the mean curvature of the level set function is $\kappa = \nabla\cdot\mathbf{n}$. In the permeable material design scenario, similarly, the periodicity of the boundary $\partial\Omega$ makes the boundary integral $\int_{\partial\Omega}\delta\varphi\tau(\varphi)B(\mathbf{u})\,d\mathbf{x}$ equal to zero in the derivation of Eq. (30). We should also note $\nabla\varphi\cdot\nabla\varphi = \|\nabla\varphi\|^2$ in Eq. (30). It is important to note that the results in Eq. (30) make the derivative sensible for periodic geometry as it is mathematically identical to the latter.

Inserting Eqs. (26)–(30) into Eq. (10) yields

$$\delta D = -\int_{\Gamma_0}\frac{\delta\varphi}{\|\nabla\varphi\|}(\lambda_0+\beta)\,d\mathbf{s} + \int_\Omega \delta\lambda_0\left(\int_\Omega H(-\varphi)\,d\mathbf{x} - V_0\right)d\mathbf{x} \tag{31}$$

where $\beta = A(\mathbf{u}) + \frac{\partial B(\mathbf{u})}{\partial\mathbf{n}} + B(\mathbf{u})\kappa + a(\mathbf{u},\mathbf{w}) + b(\mathbf{u};\mathbf{u},\mathbf{w}) - (p,\mathrm{div}\,\mathbf{w}) - (\mathbf{f},\mathbf{w})$. In order to make the total variation of the cost equation in Eq. (31) equal to zero, which is required for the optimality condition, one can set

$$\begin{aligned}
&\int_{\Gamma_0}(\lambda_0+\beta)\,d\mathbf{s} = 0\\
&\int_\Omega H(-\varphi)\,d\mathbf{x} - V_0 = 0
\end{aligned} \tag{32}$$

The first equality in Eq. (32) indicates that β should converge to a constant in the optimality condition, while the second one represents conservation of the fluid volume. Furthermore, if choose $\delta\varphi = (\lambda_0+\beta)\|\nabla\varphi\|$ in Eq. (31), we obtain

$$\delta D = -\int_{\Gamma_0}(\lambda_0+\beta)^2\,d\mathbf{s} \tag{33}$$

Then the cost function in Eq. (4) can be approximated by

$$D(t_0+\Delta t) = D(t_0) + \Delta t\delta D \Rightarrow D(t_0+\Delta t) - D(t_0) = \Delta t\delta D = -\Delta t\int_{\Gamma_0}(\lambda_0+\beta)^2\,d\mathbf{s} \leqslant 0 \tag{34}$$

This equation is of obvious importance as it ensures the dissipation of the cost function in the level set algorithm.

If the level set equation is given as

$$\delta\varphi + \mathbf{V_n}\|\nabla\varphi\| = 0 \tag{35}$$

the normal velocity can be obtained as

$$\mathbf{V_n} = -(\lambda_0 + \beta) \tag{36}$$

From the first equality in Eq. (32) we obtain the Lagrange multiplier λ_0 as below

$$\lambda_0 = -\frac{\int_{\Gamma_0} \beta \, \mathrm{d}\mathbf{s}}{\int_{\Gamma_0} \mathrm{d}\mathbf{s}} \tag{37}$$

As a result, λ_0 denotes the average value of $-\beta$ along the non-slipping boundary Γ_0, which is similar to the work in [21,34].

All the formulations presented so far are based upon the variational theory, adjoint variable technique, and Lagrangian multiplier methods, which allow us evolving the initial fluid domain via the level set method in the steepest direction to the minimum of the cost function. As a final remark in this section, the equivalence of the total variation of the cost function to zero is just one of the requirements for achieving the global minimum. A detailed discussion of its role on the minimal surface was presented in [34]. However, for the topology optimization relating to elastic and fluid continuums, the results in [20–22] and this paper indicate that it is adequate to direct the normal velocity of the level set function approaching a minimum.

3.2. Numerical implementation

The effects of several numerical issues on the implementation of the aforementioned level set model for the fluid topology optimization are discussed in this section.

3.2.1. Discretization

Two sets of meshes are presented to resolve the Hamilton–Jacobi and Navier–Stokes equations, respectively. The first mesh used for the level set function is a fixed Eulerian mesh with square elements (dashed red mesh in Fig. 2(b)). The elements in the fluid region (solid black mesh in Fig. 2(b)) can only emerge when the value of $\phi(\mathbf{x})$ at their center (red square (■) in Fig. 2(b)) is less than zero, namely the red square (■) locates within the zero-contour (green line in Fig. 2(b)) of the level set function shown as in Fig. 2(a). The mesh for fluid is just a part of the mesh imbedded in the level set mesh whose nodes (dark pentangles ★ in Fig. 2(b)) with positive $\phi(\mathbf{x})$ are not included. The motion of level set function in its normal direction triggers the changes of its zero-level contour in each iteration, making remeshing the fluid domain inevitable. This inconstant mesh in flow optimization problem is much different from its counterpart in elastic problems. In the latter, the physical properties like Young's modulus can be linearly or nonlinearly related to the value of $\phi(\mathbf{x})$ in each element. For example, the "ersatz material" with negligible Young's modulus can be used to denote void phase if $\phi(\mathbf{x}) > 0$. Thus the mesh for elastic problem can be fixed regardless the variation of the level set function $\phi(\mathbf{x})$. However, for the boundary-dependent fluid problem, assigning different viscosity to different elements is inadequate and we have to redefine the mesh of the fluid domain from time to time. Finally, to represent the boundary condition numerically, a layer of ghost elements (the outside elements in Fig. 2(b)) are added to the margin of the mesh used for the level set function.

3.2.2. Velocity extension and reinitialization

According to the level set theory [17,30], extension of the normal velocity from free boundary to a wider domain as well as reinitialization of the level set function $\phi(\mathbf{x})$ that frequently keeps itself as a signed distance function is vital in the numerical implementation. Different types of velocity extension have been studied. Here we prefer to use Eq. (8) at hand to extend normal velocity $\mathbf{V_n}$ from Γ_0 to the whole domain Ω, defined by

$$\mathbf{V_n} = -\int_{\Omega} \|\nabla\varphi\| \tau(\varphi)(\lambda_0 + \beta) \, \mathrm{d}\mathbf{x} \tag{38}$$

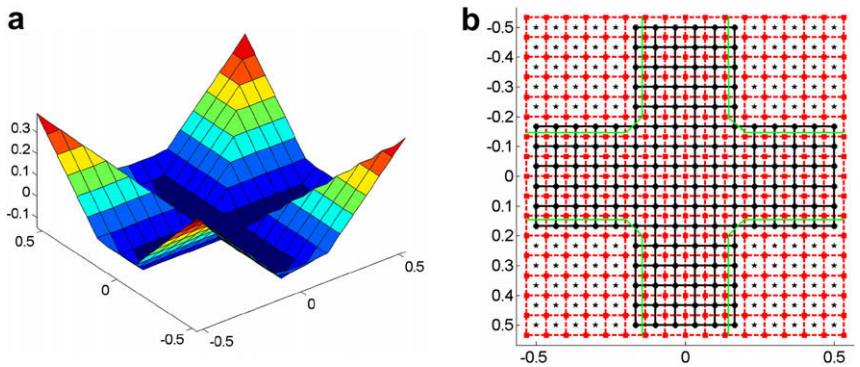

Fig. 2. Two sets of meshes for the level set $\phi(\mathbf{x})$ and fluid: (a) the level set function $\phi(\mathbf{x})$ and (b) the two set of meshes and ghost elements. (For interpretation of the references to colour in this figure legend, the reader is referred to the web version of this article.)

In addition to the velocity extension, the algorithm requires to frequently reinitialize the level set function to make the level set function a signed distance function without changing its zero-level contour. This could somewhat compromise computational efficiency, but would improve the accuracy of velocity extension, ensure the fixed thickness of the interfaces and lessen the instability of the level set function near the interface [41]. The reinitialization of the level set function is obtained by solving the Hamilton–Jacobin equation without explicitly determining the zero-level set [27],

$$\frac{\partial \varphi}{\partial t} = \mathrm{sign}(\phi)(1 - \|\nabla \varphi\|) \tag{39}$$

3.2.3. Approximation of the Heavside function and Delta function

Strict implementation of the Heavside function makes the level set algorithm singular, thus the following first-order approximation is often made [34].

$$H(\varphi) = \begin{cases} 0 & \varphi < -\eta \\ \frac{1}{2}\left(1 + \frac{\varphi}{\eta} + \frac{1}{\pi}\sin\left(\frac{\pi\varphi}{\eta}\right)\right) & \text{otherwise} \\ 1 & \varphi > \eta \end{cases} \tag{40}$$

where η is a very small but positive number defining the width of smearing functions in level set. It is easy to obtain the derivative of the Heavside function, namely the Delta function given by

$$\tau(\varphi) = \begin{cases} 0 & |\varphi| > \eta \\ \frac{1}{2\eta}\left(1 + \cos\left(\frac{\pi\varphi}{\eta}\right)\right) & \text{otherwise.} \end{cases} \tag{41}$$

3.2.4. Bisection algorithm

Since the Lagrangian multiplier in Eq. (37) comes from the first-order approximation of the cost function, it may not be sufficiently accurate and could ruin the volume constraint eventually. With an inner iteration based on the Newton method, the constraint can be pulled back onto the right track within an acceptable tolerance [34]. This method generally works fairly well except that it needs more time for stabilizing convergence due to the small move-limit imposed on the Newton method.

The bisection algorithm, which was firstly introduced to structural topology optimization in [38], enables us to quickly and easily satisfy the volume constraint. In this algorithm, the average value of the upper l_1^m (m denotes the iteration step) and lower Lagrangian multipliers l_2^m are used as the practical Lagrange multiplier $\lambda_0^m = 0.5(l_1^m + l_2^m)$ to evaluate the variation of the level set function $\delta\varphi = (\lambda_0 + \beta)\|\nabla\varphi\|$. Then an updated fluid volume V_0^{m+1} is calculated with new level set function $\varphi^{m+1} = \varphi^m + \delta\ \varphi^m$, which decides whether the upper or the lower Lagrange multiplier is reset to the last real Lagrange multiplier. That is to say, if $V_0^{m+1} \geqslant V_0^m$, then $l_1^{m+1} = \lambda_0^m$, etc. This algorithm was also reported in [33] for an elastic topology optimization model based on the radial basis functions.

4. Results and discussion

To demonstrate the above-derived mathematical model, we present in this section the topology optimization and periodic material design problems in both 2D and 3D. Unless otherwise stated, all the examples are presented in the squared

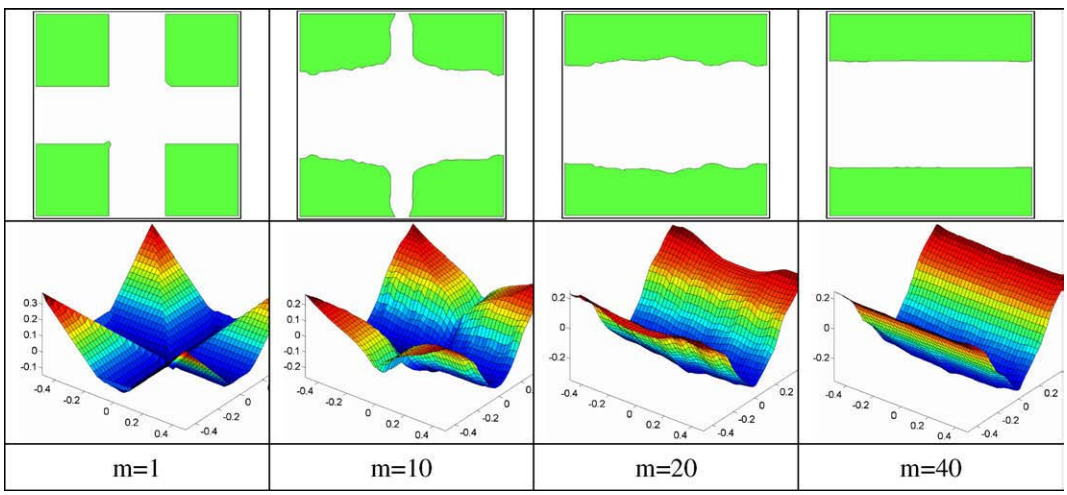

Fig. 3. Evolution process for the channel flow arriving at maximal horizontal velocity ($ny \times nx = 40 \times 40$ and m is the iteration step).

(2D) or cubic (3D) design domain whose centre is located at the origin of coordinate system. The code is developed in MATLAB and the Hamilton–Jacobian equation is solved by the program in public domain provided by Dr. Baris Sumengen (downloaded from http://vision.ece.ucsb.edu/~sumengen/).

4.1. Maximizing unidirectional permeability

The first example aims at optimizing a periodic base cell for design of 2D uniaxial permeable microstructural material. As in Fig. 3, it is expected to generate a simple straight channel capable of maximally transporting permeable fluid under a unit pressure drop in the horizontal direction. The initial fluid domain takes a Greek cross-like profile which has two vertical outputs (in the periodic boundaries) in addition to the horizontal inlet and outlet as in Fig. 1(b). The constraint of solid-fluid volume fraction is set as $V_0 = 0.5$ and the Reynolds number as $Re = 1/\mu = 1$. Terms $A(\mathbf{u})$ and $B(\mathbf{u})$ in the cost function are defined as

$$A(\mathbf{u}) = -\frac{1}{2}u_x^2 \quad B(\mathbf{u}) = 0 \tag{42}$$

where u_x is the horizontal velocity of fluid. As this problem is related to the maximization, the velocity defined in Eq. (36) for the Hamilton–Jacobi equation needs to be reversed.

Fig. 3 depicts some snapshots in the evolutions of the fluid domain (top row of the subfigures) and level set function (bottom row of the subfigures), which clearly shows that the vertical outlets are gradually bunged up and finally ended up with a straight channel in the horizontal direction. Fig. 4 shows that although the fluid volume is less than 0.5 in the beginning, it quickly converges to 0.5 (green dashed line scaled on the right vertical-axis) after few iterations. Fig. 4 also exhibits significant increase in the cost function (blue solid line scaled on the left vertical-axis), indicating a maximization process.

4.2. Maximizing bidirectional permeability

If the level set function and velocity are set square-symmetric, the design of permeable material studied in Section 4.1 becomes the maximization of 2D bidirectional permeability, which was used to derive the mathematical model in Section 3. The Reynolds number for this example remains the same as that in the previous example. The numerical results in Fig. 5 demonstrate independency of solution on the mesh size. The optimal structure is similar to those obtained from the density-based methods in [37]. It is noted that the base cell of the microstructural materials with maximal conductivity and bulk modulus has the same structures in the two dimensionality [42]. It has been also shown that the composites made of such typical microstructures are of the maximal conductivities for heat [43,44] and electricity [35], respectively.

To have a clearer view of such a porous permeable media, Fig. 6(a) illustrates the periodically materialized base cells. The horizontal velocity fields for the static Naiver–Stokes equations and their adjoint system are shown in Fig. 6(b) and (c), respectively, with arrows denoting the velocity directions.

Fig. 7 shows a more interesting design process that starts from randomly distributed solid circles. The volume of the solid phase is reset in each iteration step until it reaches 0.5. Finally the solid circles merge each other and evolve to an optimal

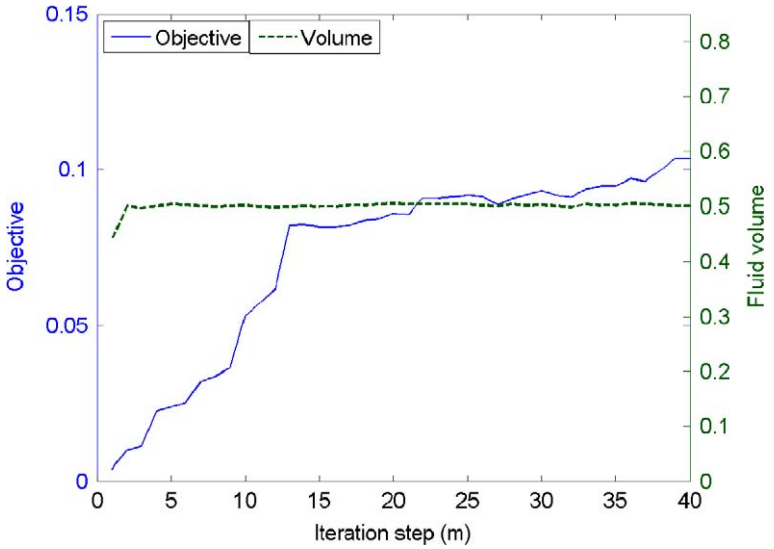

Fig. 4. Convergence of the cost function and fluid domain for the channel flow arriving at maximal horizontal transportation. (m is the iteration step). (For interpretation of the references to colour in this figure legend, the reader is referred to the web version of this article.)

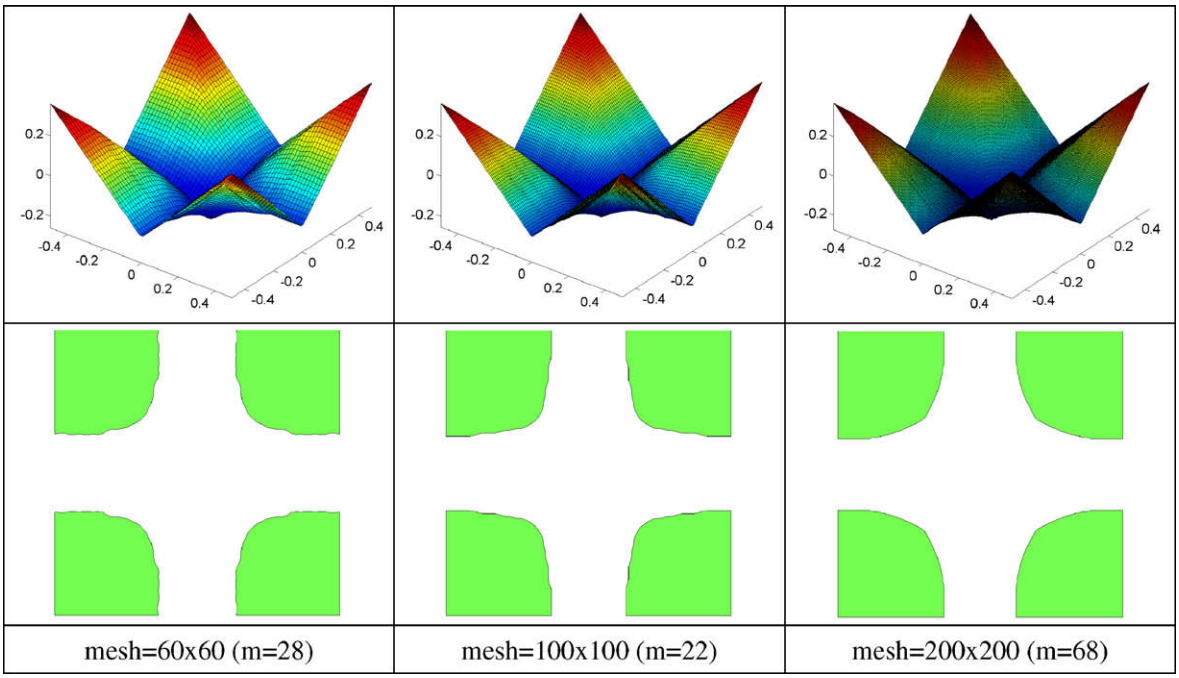

Fig. 5. Structures with maximal permeability in different mesh sizes (top, level set function; bottom fluid structures and m is the iteration step).

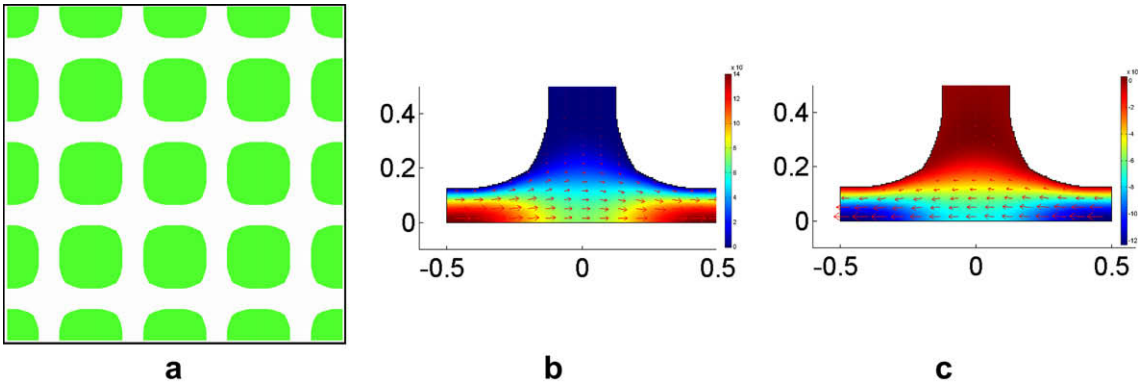

Fig. 6. Periodical extension of optimal base cell with maximal permeability and its velocity fields: (a) Periodically repeat the base cell in a 4×4 matrix form; (b) horizontal velocity distribution for the static Naiver–Stokes equation and (c) horizontal velocity distribution for the adjoint equation. ($ny \times nx = 200 \times 200$).

structure, exactly the same as the one in Fig. 5. This test well demonstrates the robustness of the level set method in handling the topological variation in the design. Fig. 8 plots the convergence histories of the fluid volume (green dashed line) and the value of the cost function (blue solid line). The red dots on the curves denote the corresponding objective values of the evolving structures in Fig. 7. It is interesting to note that there is a big jump in the cost function between iterations 540 and 650, during which the optimal crossed channel rapidly takes its final shape.

4.3. Topology optimization for minimizing energy dissipation

The abovementioned level-set procedure developed for the periodic permeable material design can be applied to general topology optimization problems in fluid mechanics. In this section, we will re-visit the design example that was previously solved by using the density-based methods in [12,14,15], where an energy dissipation involving the viscous stress is used as the cost function given by

$$A(\mathbf{u}) = \frac{1}{2}\mu\nabla\mathbf{u}\cdot(\nabla\mathbf{u}+\nabla\mathbf{u}^{\mathrm{T}}) \qquad B(\mathbf{u}) = 0 \tag{43}$$

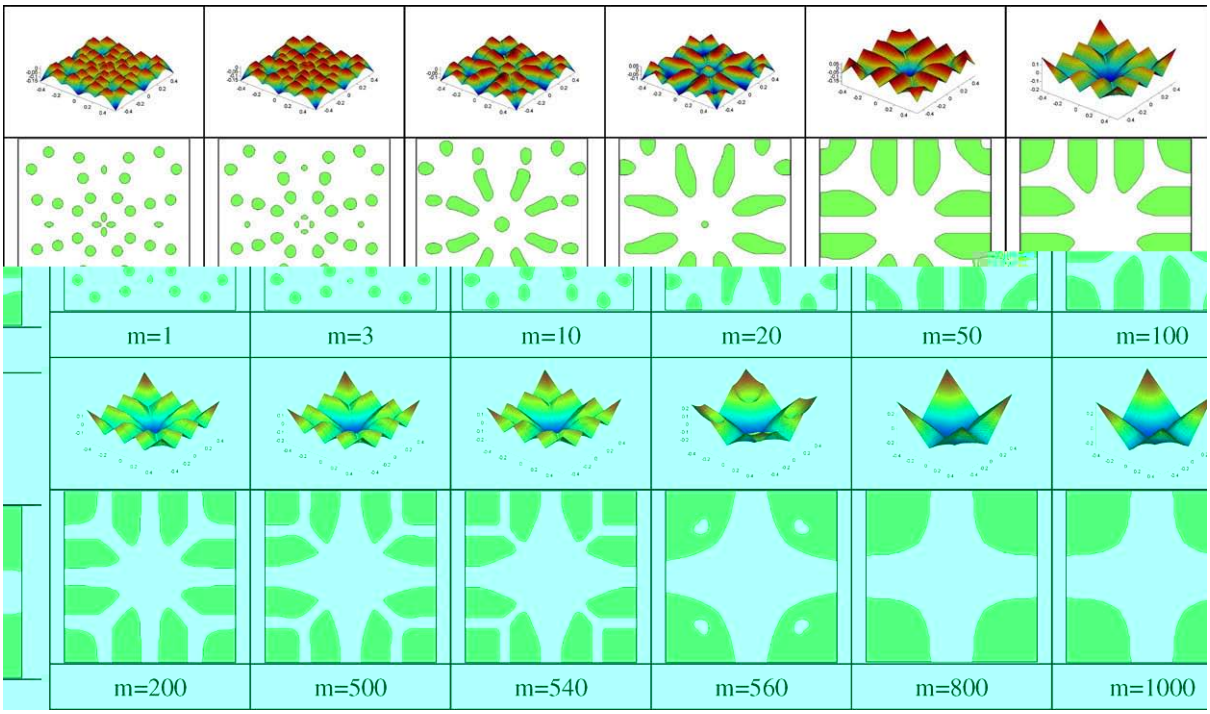

Fig. 7. Evolution process for the structure with maximal permeability flow starting from random initial values (top, level set function; bottom fluid structures and m is the iteration step $ny \times nx = 100 \times 100$).

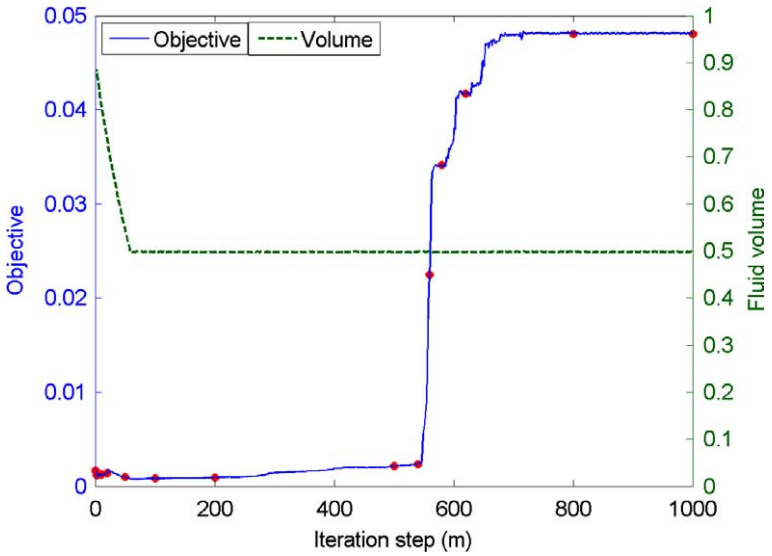

Fig. 8. Convergence of the cost function and fluid domain for the evolution of the base cell to attain maximal permeability. ($ny \times nx = 100 \times 100$ structures and m is the iteration step). (For interpretation of the references to colour in this figure legend, the reader is referred to the web version of this article.)

To understand the minimization of this cost function, we consider a square domain with a unit input velocity on the left side, free output edge (Neumann boundary) on the right side and non-slipping boundaries on the top and bottom sides, respectively. The volume fraction for the solid phase (starts from a circular shape) in the domain is maintained at 0.2. From the results shown in Fig. 9, the fluid appears washing away the solid phase from the head of circle and gradually pushes the solid phase backwards until it stops by the right boundary of the design domain. In the mean time, the solid material emerges as a bullet-like shape to minimize flow resistance. The cost function hits the minimum before majority of solid

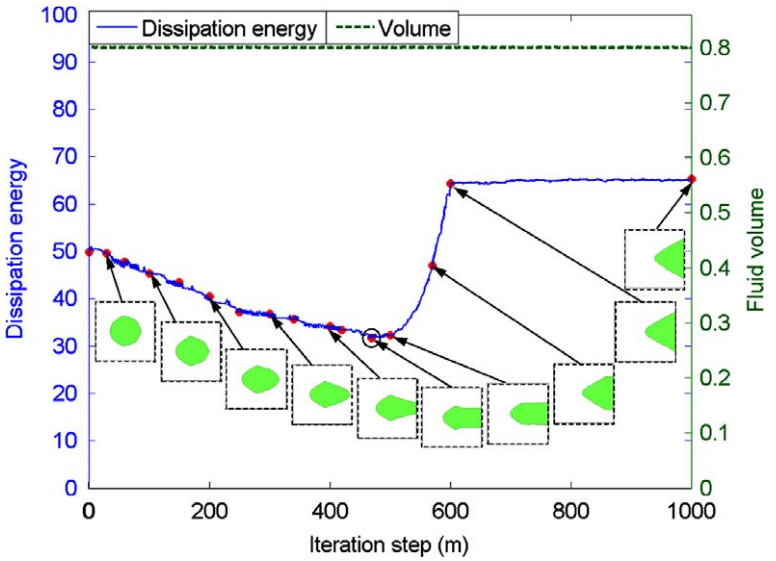

Fig. 9. Evolution process for the bullet-like structure with the minimal energy dissipation ($ny \times nx = 100 \times 100$ and Re = 1).

phase reaches the right edge. After that, as the boundary conditions are changed drastically, the cost function goes up rapidly. It is worth mentioning here that the same result can be obtained when starting the optimization procedure from a squared solid.

4.4. Topology optimization of Y-Junction for minimizing energy loss

As shown in Fig. 10b, a *Y*-Junction structure with the input and output ducts exemplifies the other topological design for minimizing the energy dissipation. The velocity at the input and output sides are ($u_x = 3$, $u_y = 0$) and ($u_x = 0$, $u_y = 1$), respectively. Volume constraint is not imposed in this example to allow the solid/fluid interface evolving more freely. Fig. 10(a) exhibits that the cost function (blue solid line) increases in the beginning as the decrease in the fluid volume (green dashed line). It is noted that after reaching the peak, the cost function turns down even when the fluid volume increases. Fig. 11(a–d) depict the evolution history, whose branching channels gradually emerge from two initial quarter-torus-like shapes (Fig. 11(a)) to a final design of straightened channels with a wider junction chamber (Fig. 11(d)). To avoid the channel being obstructed at the input boundary, where the velocity field may be trivial and so is for the cost function, two ducts are ar-

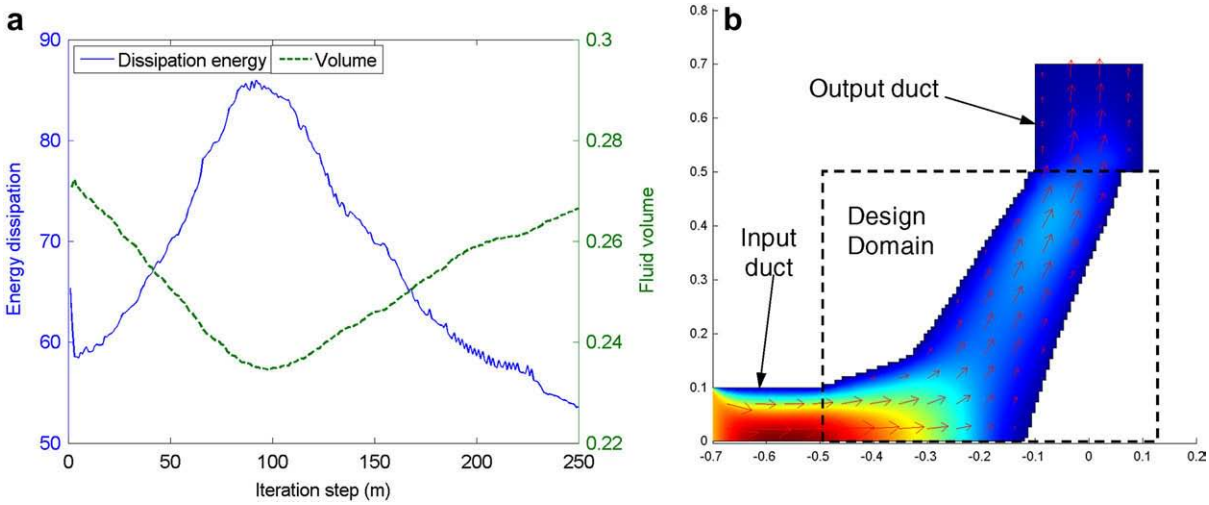

Fig. 10. Design the *T*-Junction structure (a) the variation of fluid volume and the cost function with respect to the iteration step. (b) Top part of the distribution of the horizontal velocity for static Navier–Stokes equation for the optimal structures with input and output duct ($ny \times nx = 150 \times 150$). (For interpretation of the references to colour in this figure legend, the reader is referred to the web version of this article.)

ranged to guide the inlet and outlet fluids properly (Fig. 10(b)). Such straightened design of channel is also in a good agreement with the literature [45].

4.5. Topology optimization for minimizing energy dissipation in 3D

The demand for the fluid-related shape/topology optimization in 3D is dramatically restrained by computational cost. To speed up the optimization, we simplify the governing Navier–Stokes equations to the Stokes equations by neglecting the convective term in the 3D examples below. Furthermore, to make the problems self-adjoint (the solutions to the adjoint Eq. (23) and the state Eq. (3) are the same as they have identical formulation), we only choose the dissipation energy as the objective function. In this case, the β term in the normal velocity $\mathbf{V}_n$ degenerates to

$$\beta = A(\mathbf{u}) + a(\mathbf{u},\mathbf{u}) = \mu\nabla\mathbf{u}\cdot(\nabla\mathbf{u} + \nabla\mathbf{u}^{\mathrm{T}}) \tag{44}$$

To solve for a 3D version of the example in Section 4.3, a spherical solid is considered as the initial design, which has a radius of 0.25 and locates in the centre of a cubic domain (Fig. 12). The final volume fraction is set as 0.06. On the left-hand side ($y = -0.5$ with red face), the input velocity is $u_y = 1$ and $u_x = u_z = 0$. The right-hand side of the domain ($y = 0.5$ with green face) is free surface with zero pressure $p = 0$. The other sides ($x = \pm 0.5$ and $y = \pm 0.5$ with blue faces) and the surface of the solid sphere are the non-slip boundaries with $u_x = u_y = u_z = 0$. The initial values for the level set function are set to -0.1 and 0.1 within fluid and solid regions, respectively. As can be seen in the first snapshots in Figs. 13 and 15, the initial fluid/solid surfaces are not smooth enough within a mesh of $nx \times ny \times nz = 40 \times 40 \times 40$. But as illustrated in Fig. 13, the external surface of the solid object becomes fairly smooth after a number of iterations. In the meantime, its geometry changes from sphere to rugby-like shape that appears more favorable for the flow of fluid. The gradual reduction in the energy dissipation is also seen in Fig. 14. Unlike the examples in 2D that are modeled with very fine mesh size, the conservation of the volume of solid

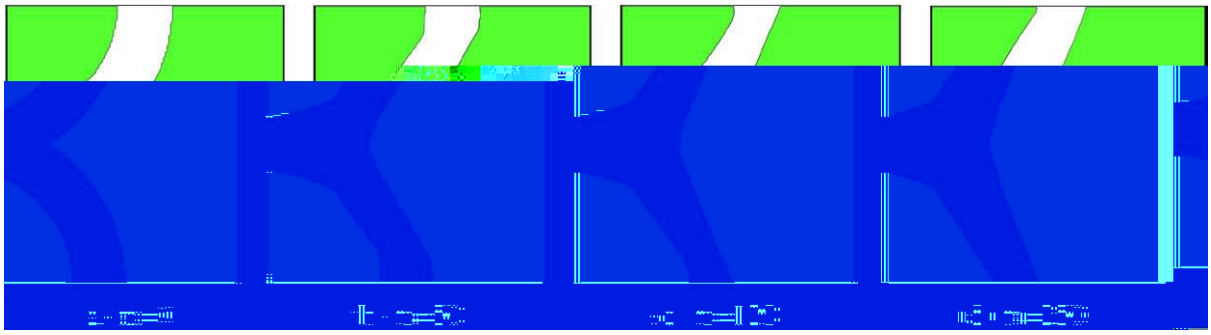

Fig. 11. Evolution of the *T*-Junction structure (m is the iteration number).

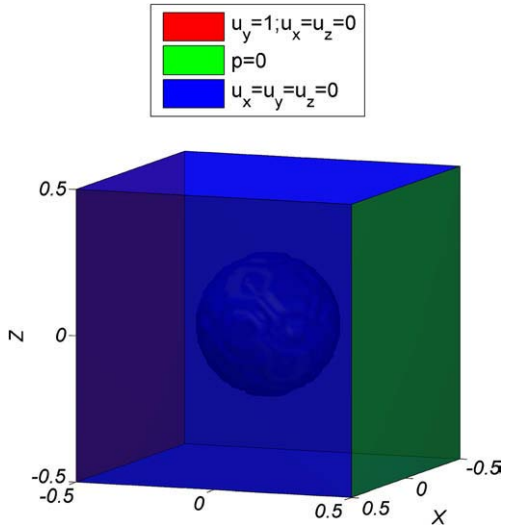

Fig. 12. A center-located solid sphere dipped in a unit cube with y-direction flow.

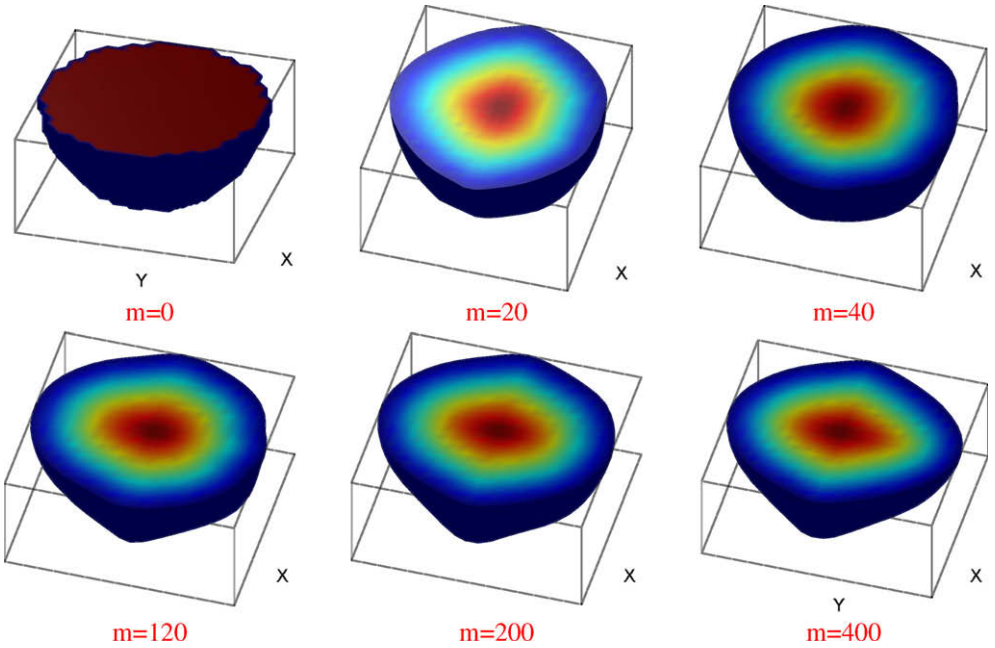

Fig. 13. The evolution snapshots of the optimized object sliced at $z = 0$.

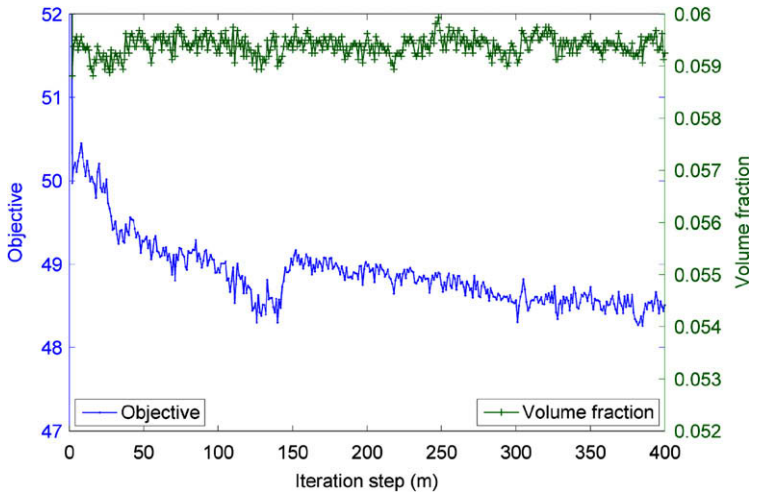

Fig. 14. The convergence of the dissipation energy and the volume fraction.

phase can not be made exactly but is within an acceptable error. To compare with the 2D results in Section 4.3, the snapshots of the evolving solid phase are plotted in y–z plane viewed from x coordinate in Fig. 15. They exhibit a similar optimization process to the steps in Section 4.3 before the object approaches to the right boundary.

4.6. 3D material design with minimal dissipation energy

Another 3D example is similar to that in Section 4.2 but the dissipation energy is used as the objective function. The initial region occupied by fluid in a unit cube is the right intersection of three identical cylinders orientated in the three coordinate axes (Fig. 16(a)), respectively. The input and output boundary conditions in y direction are the same as the example in Section 4.5 but the opposite surfaces in x and z directions are imposed the periodic boundary conditions (Fig. 16(a)). To make the microstructure equally permeable in all the three directions, the flow velocity fields (one-eighth of the cube) are cubic-symmetric. The optimization displays that the initial design with higher energy dissipation in Fig. 16(a) is progressively

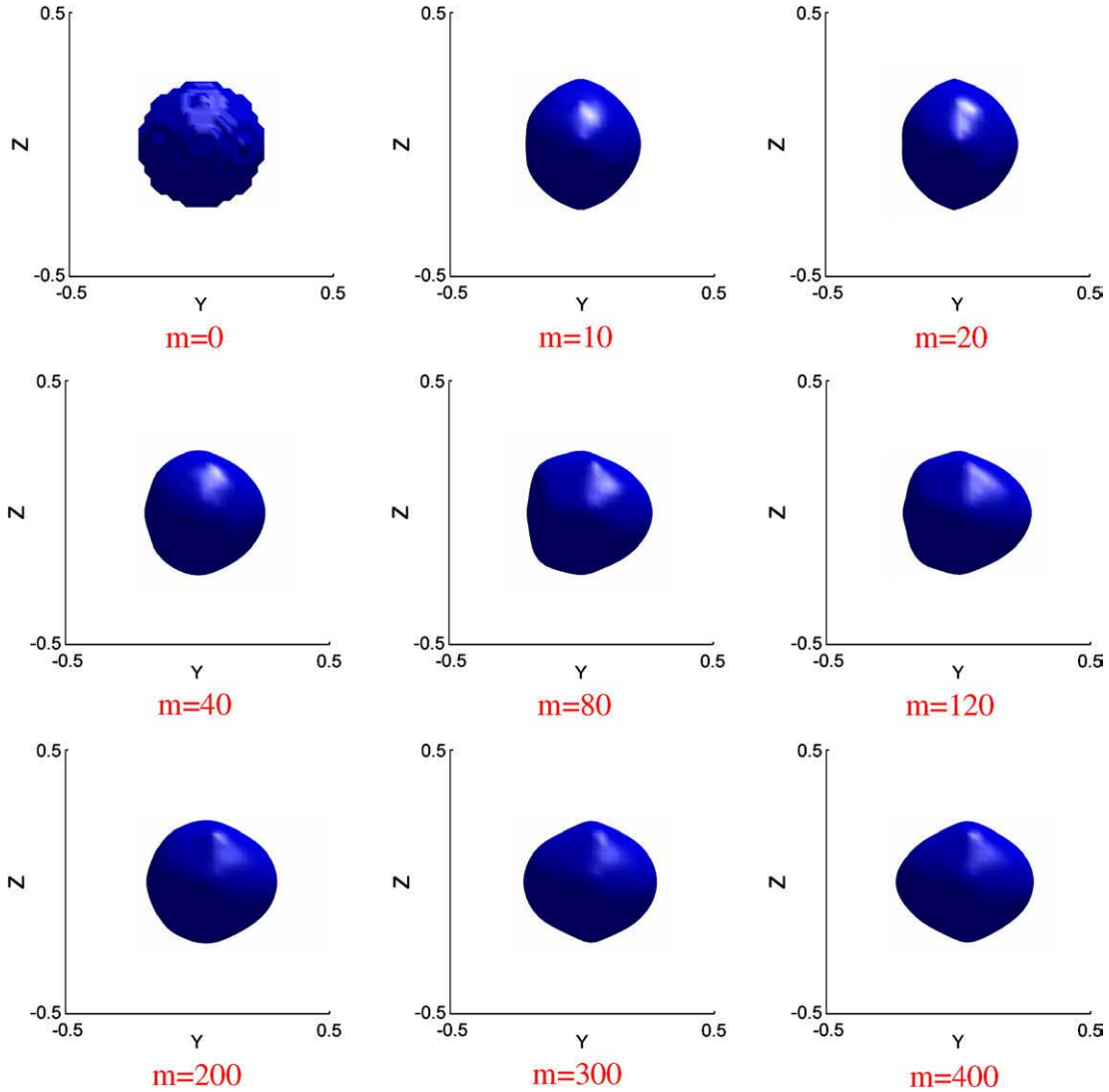

Fig. 15. The Evolution snapshots of the optimized object viewed from *x* coordinate.

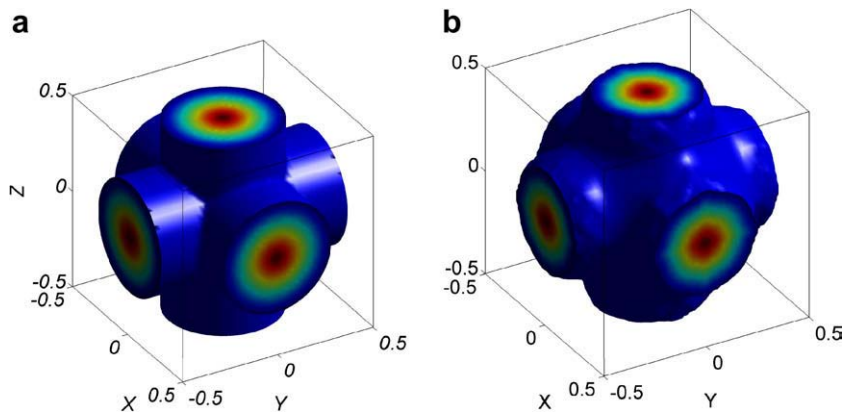

Fig. 16. A center-located solid sphere dipped in a unit cube with *y*-direction flow.

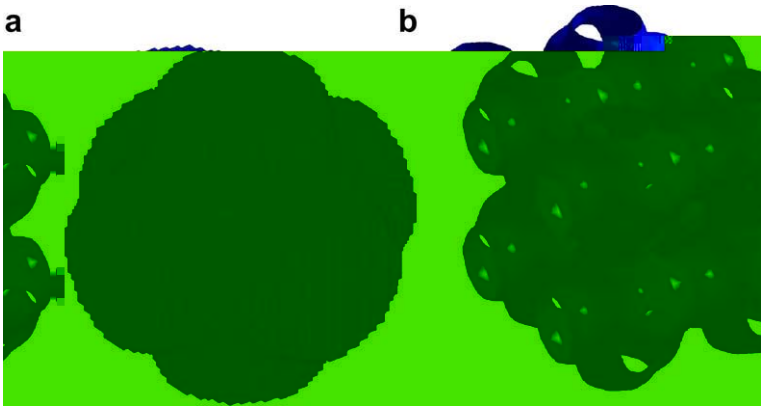

Fig. 17. Base cell and its periodically repeated structure: (a) The element-based fluid region defined by $\phi > 0$; (b) ISO surface of the periodically repeated microstructures in a $2 \times 2 \times 2$ matrix.

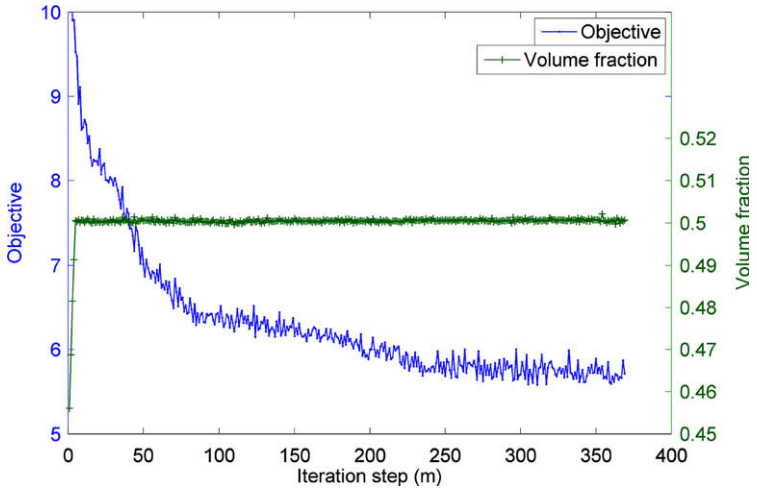

Fig. 18. The convergence of the dissipation energy and the volume fraction.

evolved to a smoother configuration in Fig. 16(b) with lower energy dissipation. Fig. 17(a) presents the fluid-occupied region within the optimal structure, which is governed by the Stokes equation in finite element analysis. Such an optimal microstructural design of solid-fluid interface is periodically repeated in Fig. 17(b). It is quite instructive to relate this interface to the well-known Schwarz P surface, on which the mean curvature equals zero everywhere. Indeed, it has been reported in literature that the composites separated by such surface have the maximum permeability [37], thermal conductivity [43], and both thermal and electrical conductivities [35]. The minimization process of the dissipation energy is plotted in Fig. 18, where the volume fraction converges to 0.5.

5. Conclusions

The level-set method has been developed in this paper to optimize the shape and topology of the fluid domain governed by the steady-state Navier–Stokes equations. Two key associative issues are clarified on (1) the expression of the solid/fluid interface via the zero-level contour of a higher-level scalar function; and (2) the derivation of the normal velocity of the level set function by means of variational calculus. The adjoint variable method is adopted to solve for the total variation of the cost function and an adjoint system of the Navier–Stokes equations is introduced.

Unlike other studies on typical elastic problems, the fluid topology optimization signified a non self-adjoint system, requiring extra effort to solve the adjoint variables. Although the Lagrange multiplier used for fluid volume constraint can be calculated explicitly, the errors due to the first-order approximation and numerical discretization can gradually violate the volume constraint. To tackle this problem a bisection technique is adopted.

All the 2D and 3D numerical experiments in both material and topological designs showed a good agreement with the results obtained by various density-based methods. The method demonstrated a great potential to deal with a broad range of fluid–solid interaction problems like vascularization.

Limitation of this model still consists in computational cost caused by the fluidic domain remeshing, velocity extension and reinitialization of the level set function. But it can be alleviated by new improvements in the level set techniques, e.g. the radial basis function as suggested in [33].

Acknowledgments

The financial support from Australian Research Council is gratefully acknowledged. The technical comments made by the anonymous reviewers and associate editor Prof. S. Osher are particularly grateful.

References

[1] O. Pironnea, Optimum profiles in Stokes flow, Journal of Fluid Mechanics 59 (1973) 117–128.
[2] O. Pironnea, Optimum design in fluid mechanics, Journal of Fluid Mechanics 64 (1974) 97–110.
[3] B. Mohammadi, O. Pironnea, Shape optimization in fluid mechanics, Annual Review of Fluid Mechanics 36 (2004) 255–279.
[4] B. Mohammadi, O. Pironnea, Applied optimal shape design, Journal of Computational and Applied Mathematics 149 (2002) 193–205.
[5] F. Baron, O. Pironnea, Multidisciplinary optimal design of a wing profile, in: Structural Optimization 93, The World Congress on Optimal Design of Structural Systems, Rio de Janeiro, Brazil, 1993, pp. 61–68.
[6] J. Reuther, A. Jameson, J. Farmer, L. Martinelli, D. Saunders, Aerodynamic shape optimization of complex aircraft congurations via an adjoint formulation, Aerospace Letters (AIAA) 96 (1996) 0094.
[7] J.J. Reuther, A. Jameson, J.J. Alonso, M.J. Rimlinger, D. Saunders, Constrained multipoint aerodynamic shape optimization using an adjoint formulation and parallel computers, part 1, Journal of Aircraft 36 (1999) 51–60.
[8] J.J. Reuther, A. Jameson, J.J. Alonso, M.J. Rimlinger, D. Saunders, Constrained multipoint aerodynamic shape optimization using an adjoint formulation and parallel computers, part 2, Journal of Aircraft 36 (1999) 61–74.
[9] L. Tartar, Control problems in the coefficients of PDE, in: A. Bensoussan (Ed.), Lecture notes in Economics and Math systems, vol. 107, Springer, Berlin, 1974, pp. 420–426.
[10] G.P. Steven, Q. Li, Y.M. Xie, Evolutionary topology and shape design for general physical field problems, Computational Mechanics 26 (2000) 129–139.
[11] Y.M. Xie, G.P. Steven, A simple evolutionary procedure for structural optimization, Computers and Structures 49 (1993) 885–896.
[12] T. Borrvall, J. Petersson, Topology optimization of fluids in Stokes flow, International Journal for Numerical Methods in Fluids 41 (2003) 77–107.
[13] M.P. Bendsøe, O. Sigmund, Topology Optimization: Theory, Methods, and Applications, Springer, Berlin, New York, 2003.
[14] L.H. Olesen, F. Okkels, H. Bruus, A high-level programming-language implementation of topology optimization applied to steady-state Navier–Stokes flow, International Journal for Numerical Methods in Engineering 65 (2006) 975–1001.
[15] A. Gersborg-Hansen, O. Sigmund, R.B. Haber, Topology optimization of channel flow problems, Structural and Multidisciplinary Optimization 30 (2005) 181–192.
[16] N. Wiker, A. Klarbring, T. Borrvall, Topology optimization of regions of Darcy and Stokes flow, International Journal for Numerical Methods in Engineering 69 (2007) 1374–1404.
[17] S. Osher, J.A. Sethian, Front propagating with curvature dependent speed: algorithms based on Hamilton–Jacobi formulations, Journal of Computational Physics 78 (1988) 12–49.
[18] D.L. Chopp, Computing minimal-surfaces via level set curvature flow, Journal of Computational Physics 106 (1993) 77–91.
[19] R. Malladi, J.A. Sethian, Image-processing via level set curvature flow, in: Proceedings of the National Academy of Sciences of the United States of America, vol. 92, 1995, pp. 7046–7050.
[20] J.A. Sethian, A. Wiegmann, Structural boundary design via level set and immersed interface methods, Journal of Computational Physics 163 (2000) 489–528. Sep. 20.
[21] M.Y. Wang, X.M. Wang, D.M. Guo, A level set method for structural topology optimization, Computer Methods in Applied Mechanics and Engineering 192 (2003) 227–246.
[22] G. Allaire, F. Jouve, A.M. Toader, Structural optimization using sensitivity analysis and a level-set method, Journal of Computational Physics 194 (2004) 363–393.
[23] Y.L. Mei, X.M. Wang, A level set method for microstructure design of composite materials, Acta Mechanica Solida Sinica 17 (Sep) (2004) 239–250.
[24] M.Y. Wang, X.M. Wang, A level-set based variational method for design and optimization of heterogeneous objects, Computer-Aided Design 37 (Mar) (2005) 321–337.
[25] F. Santosa, A level-set approach for inverse problems involving obstacles, Control Optimisation Calculas of Variation 1 (1996).
[26] M. Burger, S.J. Osher, A survey in mathematics for industry – A survey on level set methods for inverse problems and optimal design, European Journal of Applied Mathematical 16 (April) (2005) 263–301.
[27] M. Sussman, P. Smereka, S. Osher, A level set approach for computing solutions to incompressible 2-phase flow, Journal of Computational Physics 114 (1994) 146–159.
[28] H.K. Zhao, T. Chan, B. Merriman, S. Osher, Variational level set approach to multiphase motion, Journal of Computational Physics 127 (Aug) (1996) 179–195.
[29] S. Osher, R.P. Fedkiw, Level set methods: An overview and some recent results, Journal of Computational Physics 169 (2001) 463–502.
[30] J.A. Sethian, Level Set Methods and Fast Marching Methods, Cambridge University Press, New York, 1999.
[31] S.J. Osher, F. Santosa, Level set methods for optimization problems involving geometry and constraints I. Frequencies of a two-density inhomogeneous drum, Journal of Computational Physics 171 (2001) 272–288. Jul 20.
[32] M.Y. Wang, X.M. Wang, PDE-driven level sets, shape sensitivity and curvature flow for structural topology optimization, CMES-Computer Modeling in Engineering and Sciences 6 (2004) 373–395.
[33] S.Y. Wang, K.M. Lim, B.C. Khoo, M.Y. Wang, An extended level set method for shape and topology optimization, Journal of Computational Physics 221 (2007) 395–421.
[34] Y. Jung, K.T. Chu, S. Torquato, A variational level set approach for surface area minimization of triply-periodic surfaces, Journal of Computational Physics 223 (2007) 711–730.
[35] S. Torquato, S. Hyun, A. Donev, Multifunctional composites: optimizing microstructures for simultaneous transport of heat and electricity, Physical Review Letters 89 (2002).
[36] X.B. Duan, Y.C. Ma, R. Zhang, Optimal shape control of fluid flow using variational level set method, Physics Letters A 372 (2008) 1374–1379. Feb 25.
[37] J.K. Guest, J.H. Prévost, Design of maximum permeability material structures, Computer Methods in Applied Mechanics and Engineering 196 (2007) 1006–1017.
[38] O. Sigmund, A 99 line topology optimization code written in Matlab, Structural and Multidisciplinary Optimization 21 (2001) 120–127.

[39] Y. Jung, S. Torquato, Fluid permeabilities of triply periodic minimal surfaces, Physical Review E 72 (2005) 056319.
[40] F. Murat, S. Simon, Etudes de problemes d'optimal design, Springer-Verlag, Berlin, 1976.
[41] J.A. Sethian, P. Smereka, Level set methods for fluid interfaces, Annual Review of Fluid Mechanics 35 (2003) 341–372.
[42] N.d. Kruijf, S.W. Zhou, Q. Li, Y.W. Mai, Topological design of conductive structures, International Journal of Solids and Structures 44 (2007) 7092–7109.
[43] S.W. Zhou, Q. Li, The relation of constant mean curvature surfaces to multiphase composites with extremal thermal conductivity, Journal of Physics D: Applied Physics 40 (2007) 6083–6093.
[44] V.J. Challis, A.P. Roberts, A.H. Wilkins, Design of three dimensional isotropic microstructures for maximized stiffness and conductivity, International Journal of Solids and Structures 45 (2008) 4130–4146.
[45] E. Katamine, T. Tsubata, H. Azegami, Solution to shape optimization problem of viscous flow fields considering convection term, in: M. Tanaka, G.S. Dulikravich (Eds.), Inverse Problems in Engineering Mechanics, vol. IV, Elsevier Science, 2003, pp. 401–408.